Biosensors and Bioelectronics 137 (2019) 45–51

Contents lists available at ScienceDirect

Biosensors and Bioelectronics

journal homepage: www.elsevier.com/locate/bios

A novel label-free strategy for the ultrasensitive miRNA-182 detection based on MoS_2/Ti_3C_2 nanohybrids

Lei Liu*,[1], Yumin Wei[1], Songlong Jiao, Songyang Zhu, Xiaolin Liu

Jiangsu Key Laboratory for Design and Manufacture of Micro-Nano Biomedical Instruments, School of Mechanical Engineering, Southeast University, Nanjing, 211189, People's Republic of China

ARTICLE INFO

Keywords:
MiRNA
Lung cancer
MoS_2
MXenes

ABSTRACT

MicroRNAs (miRNAs) are regarded as a large variety of cancer-related biomarkers, and they have attracted wide attentions in recent years. In this work, a novel label-free strategy for the ultrasensitive detection of miRNA-182 (a typical biomarker for lung cancer) based on MoS_2/Ti_3C_2 nanohybrids was suggested. Firstly, modified glassy carbon electrode (GCE) with massive active sites and good electronic conductivity was prepared for biosensing. Then, based on this platform a descent signal in differential pulse voltammetry (DPV) peak current could be observed with the addition of probe RNA with negative charge. Thereafter, with the hybridization of target miRNA-182 with immobilized probe RNA and the swelling-induced breakage of Au–S bonds between RNA and the electrode surface, the characteristic DPV signals increase were found. In particular, this biosensing platform for special miRNAs possessed a good linear detection window in a range from 1 fM to 0.1 nM with a detection limit of 0.43 fM.

1. Introduction

Cancer endangers human health seriously. It is reported that there are about 18.1 million new cases of cancer and approximately 9.6 million malignant tumor deaths globally by 2018. Particularly, lung cancer is a disease with the highest morbidity and mortality in malignancy, and its early and effective diagnosis is of great importance and necessity (Bray et al., 2018). Compared with traditional detection methods (chemotherapy, X-ray, computed positron emission topographies and optical coherence etc.), ultrasensitive detection of cancer-related biomarkers seems to be more competitive and more promising in its early diagnosis (Roointan et al., 2018). As a kind of typical cancer-related biomarkers, miRNAs are a set of short non-coding RNA molecules with about 18–25 nucleotides, which play a vital role in plants and animals by influencing cell differentiation, proliferation and survival (Zhu et al., 2011; Rupaimoole and Slack, 2017; Tian et al., 2018). For example, miRNA-182 shows tissue specificity and sequential expression in the different stages during lung cancer development or evolution (Li et al., 2018a, 2018b; Miko et al., 2009). Additionally, a large number of stable miRNAs have been found in human serum and plasma, showing good accessibility and convenience of miRNAs detection (Zhao et al., 2010; Resnick et al., 2009; Chen et al., 2008).

Based on the rapid developments of material science, two-dimensional (2-D) films or flakes (such as graphene, transition metal dichalcogenides and black phosphorus) are applied to detect molecular biomarkers due to their large surface area, low biotoxicity, exceptional biocompatibility and anisotropic electron transporting (Ji et al., 2017; Kalantar-zadeh and Ou, 2015; Tan et al., 2017; Ryoo et al., 2013; Dong et al., 2012; Chen et al., 2017). Recently, 2-D transition metal carbides/carbonitrides (MXenes), which are produced by etching of the A-layers from $M_{n+1}AX_n$ (MAX) phases selectively (Lin et al., 2016a), have been revealed as a potential solution for ultrasensitive biosensors, although only little research has been reported on the detection of miRNAs by MXenes (Ti_3C_2) till now. Furthermore, combining 2-D layered materials with other nanomaterials can achieve better detection by synergetic effect, such as biofunctionalized 2-D MXenes (Ti_3C_2) being used to detect cancer-related biomarker CEA (Kumar et al., 2018; Gan et al., 2017), MoS_2 nanosheets functionalized by poly-xanthurenic acid film being used for signal amplification (Zhang et al., 2018; Shuai et al., 2017). Most of these studies focused on increasing its surface area to improve the electron transfer properties and active sites on the surface, since the electron transfer events occurr at higher rates at the edge surface than the basal surface (Chia et al., 2015). In fact, the electrochemical performance of Ti_3C_2 is unstable, resulting from its surface functional groups (-F, –OH, =O) introduced in its preparation (Fig. S2). Relevant in-depth research is necessary, and exploring novel strategy

* Corresponding author.
E-mail address: liulei@seu.edu.cn (L. Liu).
[1] These authors contributed equally to this work.

https://doi.org/10.1016/j.bios.2019.04.059
Received 31 January 2019; Received in revised form 26 April 2019; Accepted 30 April 2019
Available online 01 May 2019
0956-5663/

for Ti_3C_2-based miRNA detection may be meaningful and attractive.

In this study, MoS_2/Ti_3C_2 nanohybrids were prepared and attempted to use for the ultrasensitive detection of miRNA-182, while the effective detection range and sensitivity have also been investigated.

2. Experimental sections

2.1. Materials and instruments

Lithium fluoride (LiF) and Ethylene glycol were obtained from Nanjing Chemical Reagent Co., Ltd. (Nanjing, China). Hydrochloric acid (HCl), ethylenediaminetetraacetic acid (EDTA), potassium chloride (KCl) and Thiourea ($SC(NH_2)_2$) were purchased from Shanghai Lingfeng Chemical Reagent Co., Ltd. (Shanghai, China). Gamma alumina powder (particle size ≤ 0.05 μm) was bought from CH Instruments, Inc. (USA). Gold Nano-particles (AuNPs, particle size ≤ 20 nm) and ammonium molybdate tetrahydrate ($(NH_4)_6Mo_7O_{24}.4H_2O$) were purchased from Shanghai Maclean Biochemical Technology Co., Ltd. (Shanghai, China). Bovine serum albumin (BSA) was purchased from Shanghai Yuanye Biological Technology Co., Ltd. (Shanghai, China). Diethyl pyrocarbonate (DEPC) water was bought from Hefei Xinenyuan Biotechnology Co., Ltd. (Hefei, China). Magnesium chloride ($MgCl_2$) and calcium chloride ($CaCl_2$) were bought from Xilong Science Co., Ltd. Potassium hexacyanoferrate (III) ($K_3Fe(CN)_6$, ≥99.5%) was purchased from Aladin. Potassium hexacyanoferrate (II) trihydrate ($K_4Fe(CN)_6{\bullet}3H_2O$, ≥99.5%), tris(hydroxymethyl)aminomethane (Tris) and sodium chloride (NaCl) were obtained from Shanghai Sinopharm Group (Shanghai, China). All vessels and tips were soaked in DEPC water for 24 h before being used to minimize the effect of RNase on miRNAs stability. All the oligonucleotides were synthesized by Shanghai Sangon Biological Engineering Technology Co. Ltd. (Shanghai, China) and their sequences were as follows:

Probe RNA: 5′–SH–$(CH_2)_6$ -UUU UUA GUG UGA GUU CUA CCA UUG CCA AA-3'.

MiRNA-182: 5′-UUU GGC AAU GGU AGA ACU CAC ACU-3'.

Single-base mismatch: 5′-UUU GGC AAU GGU CGA ACU CAC ACU-3′

Three-base mismatch: 5′-GUU GGC AAU AGU AGA ACU CAC AAU-3′

All solutions used in this work were formulated from DEPC water. The stock solution of probe RNA was prepared in SSPE buffer containing 0.02 M EDTA, 2.98 M NaCl and 0.20 M phosphate buffer (20 × diluted, pH = 7.4). The stock solution of miRNA-182 was prepared in Tris-HCl, including 0.02 M Tris, 0.14 M NaCl, 0.001 M $MgCl_2$, 0.005 M KCl and 0.001 M $CaCl_2$ (pH = 7.4). The rinsing solution was mixed phosphate buffer (PBS, pH = 7.4). All solutions and oligonucleotide were kept at −4 °C.

Scanning electron microscope (SEM, Inspect F50, FEI), transmission electron microscopy (TEM, G220, FEI) and X-ray diffraction (XRD, Smartlab-3, Rigaku) were used to observe the morphologies and crystal structures of MoS_2/Ti_3C_2 nanohybrids. Ultra-pure water used in this work was provided by an UPT- II-10T water purifier (Xi'an Youpu Instrument Equipment Co., Ltd.). XPS characterizations were acquired on a PHI Quantera II Scanning XPS Microprobe spectrometer with Al Ka monochrome X-rays ($h\nu$ = 1486.6 eV) source. All the binding energies of the XPS spectra were reference to C 1s peak at 284.8 eV. Electrochemical measurements were performed on a CHI660E electrochemical workstation (Shanghai Chenhua Instruments, China). A conventional three-electrode system, consisting of GCE with the diameter of 3.0 mm, an Ag/AgCl electrode as reference electrode and a platinum wire auxiliary electrode was used in all electrochemical measurements. The involved electrochemical techniques were cyclic voltammetry (CV), A.C. impedance (EIS) and differential pulse voltammetry (DPV). All the electrochemical measurements were operated in PBS buffer (pH = 7.4), containing 0.1 M KCl and 2.5 mM $[Fe(CN)_6]^{3-/4-}$.

2.2. Preparation of MoS_2/Ti_3C_2 nanohybrids

Layered Ti_3C_2 was synthesized by a modified chemical exfoliation method according to previous reports (Naguib et al., 2011; Lin et al., 2016b). Briefly, 1.98 g LiF was dispersed in HCl (30 mL, 6 M). Then 3.00 g Ti_3AlC_2 powder was added and etched for 3 days under magnetic stirring. After etching, it was washed with water and ethanol, separated by centrifugation. Finally, the cleaned powder was dried at 80 °C for 10 h.

MoS_2/Ti_3C_2 nanohybrids were prepared via a hydrothermal method (Liu et al., 2018). 0.80 g $(NH_4)_6Mo_7O_{24}$ $4H_2O$ and 1.80 g $SC(NH_2)_2$ were dispersed in 24 mL deionized water, and the mixture was sonicated for 30 min. Then, 50 mg Ti_3C_2 powder was added into the mixture, followed by a 30-min ultrasonication. After that, the mixture was transferred into a 50 mL polytetrafluoroethylene-lined stainless steel autoclave and was heated to 200 °C for 10 h. After cooling to room temperature, it was washed with water and ethanol, separated by centrifugation. The product was dried at 80 °C for 10 h.

2.3. Fabrication of biosensing platform

Fig. 1 shows the fabrication process of the biosensing platform for the detection of miRNA-182 (BSA/ssRNA/AuNPs/MoS_2/Ti_3C_2/GCE): 7.5 mg MoS_2/Ti_3C_2 powder was dispersed in 5 mL deionized water by ultrasonication for 30 min to get uniform suspension (1.5 mg mL^{-1}). Prior to use, bare GCE was sanded with 0.05 μm alumina slurry on a clean flannel until a mirror-like surface was obtained. Successively, it was sonicated in mixture of ethanol and deionized water for 5 min to remove adhered alumina particles, rinsed with DEPC water and dried under nitrogen flow. 10 μL MoS_2/Ti_3C_2 suspensions was dripped onto the pretreated GCE and dried to obtain a MoS_2/Ti_3C_2 film at 35 °C. Afterwards, 10 μL AuNPs solution was added onto the electrode surface and dried at room temperature. The obtained electrode was noted as AuNPs/MoS_2/Ti_3C_2/GCE. When the MoS_2/Ti_3C_2 suspensions were transferred to the dried surface of GCE, a continuous uniform film was formed on the electrode surface. The nanohybrids were immobilized on the surface of the electrode by van der Waals force and electrostatic action, and Au atoms were adsorbed on MoS_2/Ti_3C_2 nanohybrids by weak van der Waals through dripping solutions with AuNPs on the electrode surface. Moreover, Au was adsorbed on the top site directly above a Mo atom (Li et al., 2015).

After that, 10 μL probe RNA solution was dripped onto AuNPs/MoS_2/Ti_3C_2/GCE and then dried at room temperature. The modified electrode was washed with PBS solution (pH = 7.4) to remove unbound ssRNA, 50 μL of 1% BSA was dripped onto ssRNA/AuNPs/MoS_2/Ti_3C_2/GCE for 40 min to block unbound gold particles surface and avoid non-specific adsorption. Then, the electrode was rinsed by PBS solution (pH = 7.4) again. Finally, the resulting electrode was used for the detection of miRNA-182.

3. Results and discussion

3.1. Characterization of nanohybrids for biosensing

SEM image (Fig. 2A) shows the compact microstructure of solid Ti_3AlC_2, where there is no gap between layers. Therefore, Ti_3AlC_2 possessed low active sites as an adsorption substrate. After etching Al by HF, Ti_3C_2 (Fig. 2B) exhibits a lot of loose structures compared with Ti_3AlC_2. The spacing between the slices was significantly enlarged. SEM image of MoS_2/Ti_3C_2 nanohybrids (Fig. 2C and the inserted image) indicates that the flower-like substance is uniformly distributed between Ti_3C_2 layer and surface. The thickness of nanosheet was about 20 nm, and flower-like MoS_2 grew vertically around the layered Ti_3C_2.

After a 24-h hydrothermal treatment at 200 °C, small parts of Ti_3C_2 were oxidized to TiO_2, but the obtained Ti_3C_2 still maintained good layered structure (Fig.2E and Fig. S1). HR-TEM image of MoS_2/Ti_3C_2

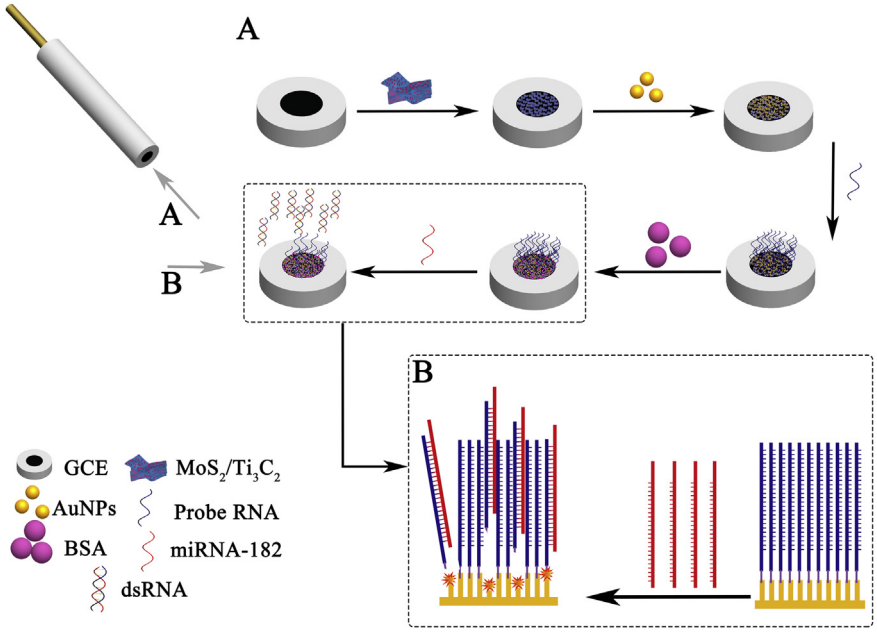

Fig. 1. The schematic of sequent steps of nanobisensor fabrication and detection (A). The explanation of the swelling-induced Au–S bond breakage (B).

nanohybrids (Fig. 2D) illustrates the lattice structure of MoS_2 and the layer-to-layer spacing of MoS_2. It indicated that the pitch of (002) peak plane was about 0.62 nm, which was consistent with the theoretically calculated value (Joly-Pottuz et al., 2005). The formation of MoS_2/Ti_3C_2 nanohybrids was also confirmed by XRD (Fig. 2E). After HF-etching, the most intense XRD peak of Ti_3AlC_2 at 38° disappeared. After the aluminum atomic layer was extracted to form lamellar titanium carbide, only the peak at 6° was still significant. Compared with MoS_2 powder formed by direct hydrothermal method, XRD spectrum for MoS_2/Ti_3C_2 nanohybrids also shows a MoS_2 characteristic peak at 14°. In addition, layered Ti_3C_2 provided enough spatial loci for MoS_2 growth and great electronic conductivity for the nanohybrids. By simple hydrothermal method, layered Ti_3C_2 surface was covered uniformly by vertical MoS_2 nanosheets with a size of ~100 nm.

3.2. Electrochemical biosensing platform

As shown in Fig. 1A, MoS_2/Ti_3C_2 nanohybrids were added onto the GCE surface by simple drop casting method, which intended to enlarge the specific surface area and broadened the junction area of the

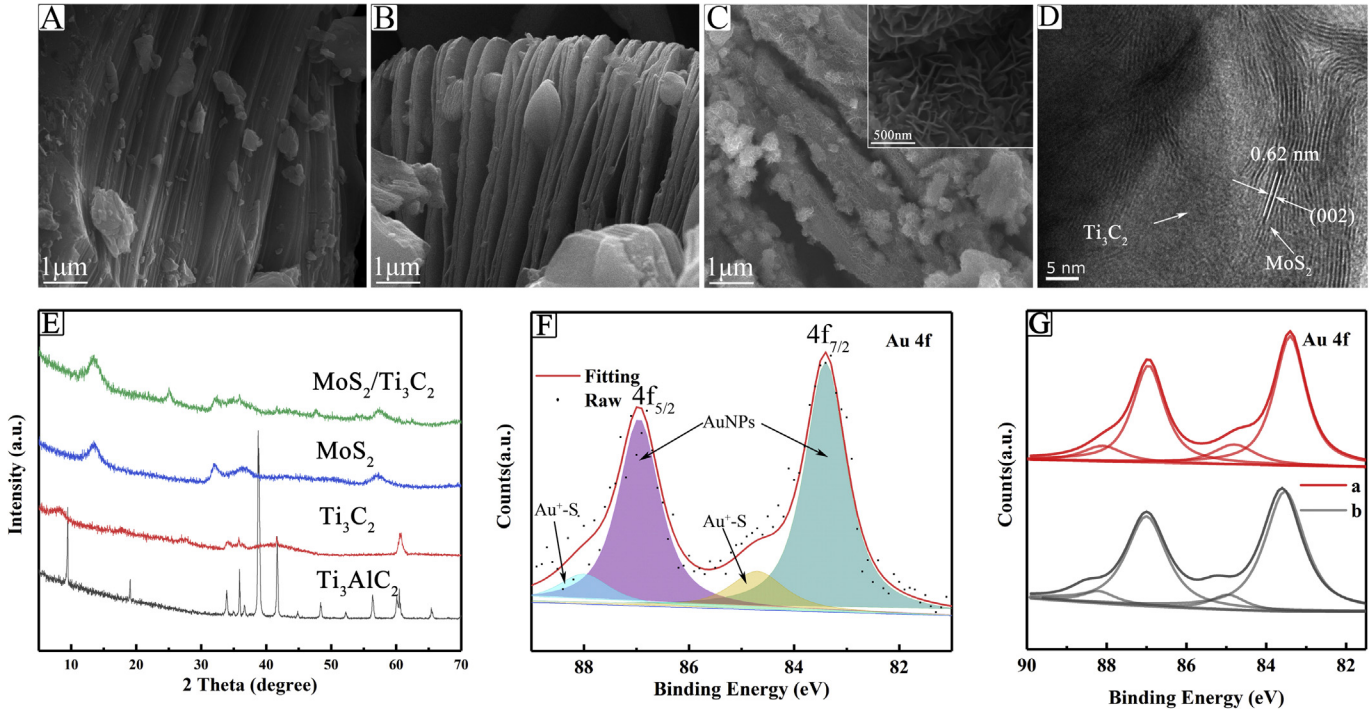

Fig. 2. SEM image of original Ti_3AlC_2 (A), Ti_3C_2 after HF etching (B) and MoS_2/Ti_3C_2 (C). HR-TEM image of MoS_2/Ti_3C_2 nanohybrids (D). XRD image of original Ti_3AlC_2, Ti_3C_2, MoS_2 and MoS_2/Ti_3C_2 (E). X-ray photoelectron spectra of Au 4f on modified electrode (F) and the comparison XPS spectra of AuNPs: without Au–S bond breakage(G-a) and with Au–S bond breakage partly(G-b).

electrode/electrolyte. Combining the high electronic conductivity and stable electrochemical performance, MoS_2/Ti_3C_2 nanohybrids showed better electronic conductivity, higher specific surface area, more active sites and excellent electrochemical performance. In order to enlarge the immobilization of probe RNA (ssRNA) on the electrode surface, AuNPs are introduced through electrostatic adsorption. Then, AuNPs were introduced to the surface of MoS_2/Ti_3C_2/GCE (Fig. S3) to amplify the electrochemical signal and reduce the R_{ct}. AuNPs provided Au atoms to form Au–S bonds with –SH modified ssRNA, and the probe RNA was immobilized on the AuNPs/MoS_2/Ti_3C_2/GCE by Au–S bonds. Numerous studies have shown that ssRNA is negatively charged through its phosphate backbone, which weakens the electrochemical signal because the redox probe $[Fe(CN)_6]^{3-/4-}$ is also charged negatively. Due to MoS_2 grown vertically on the surface of layered Ti_3C_2, the edge surface was exposed absolutely and Au–S bonds were approaching saturation. That meant the large grafting density of Au–S bonds, which induced the critical dry thickness decreasing. With the addition of miRNA-182, the dry thicknesses of dsRNA films exceeded the critical dry thickness. Then, swelling-induced Au–S bond breakage occurred and dsRNA was released from the electrode surface (Lv et al., 2014) (Fig. 1B). Finally, the amount of ssRNA was decreasing with the release amount of dsRNA, consistent with the addition of target miRNA-182. Accordingly, the electrochemical biosensor based on MoS_2/Ti_3C_2 nanohybrids was established successfully.

X-ray photoelectron Au 4f spectra of AuNPs and Au–S bond are presented in Fig. 2F and G, which are characteristic of predominant metallic gold with the Au $4f_{7/2}$ binding energy of 83.60 ± 0.05 eV, and its relative intensity correlated with AuNPs of about 20 nm. A line at 85.00 ± 0.05 eV that corresponded to Au(I) atoms bonded to S of probe RNA, which revealed the content of Au–S bond [Mikhlin et al., 2010]. Fig. 2G gives the comparison of the XPS spectra for Au 4f before and after the addition of target miRNA-182. The ratios of peak areas of the line at 85.0 ± 0.05 eV and the one at 83.6 ± 0.05 eV were 20.31% and 13.30% respectively. It showed the peak intensity and area corresponding to Au(I) decreased after the addition of miRNA-182. The result illustrated the occurrence of Au–S bond formation with the addition of probe RNA and Au–S bond breakage with the addition of target miRNA-182.

The CV and EIS were used to electrochemically evaluate the electrode surface performance during the modified process and monitor the electron transfer properties under a standard redox system. According to the CV plot, the bare GCE (Fig. 3A, **curve a**) displayed excellent redox peaks. The peak-to-peak potential separation was about 100 mV, which verified good performance of the electrochemical three-electrode system. Compared with bare GCE, the electrodes modified with MoS_2/Ti_3C_2 (Fig. 3A, **curve b**) and AuNPs (Fig. 3A, **curve c**) showed increased cathodic/anodic currents, which revealed that the modification of GCE was successful. The corresponding EIS data were also consistent with CV curve. Randle's equivalent circuit (inserted image in Fig. 3B) was chosen to simulate the physico-chemical process occurring at the electrode surface (Panagopoulou et al., 2010). Nyquist spectra was plotted to describe the EIS data. The electron transfer resistance (R_{ct}) and the diffusion limited procedure (Suni, 2008) were characterized by the diameter of the semicircle and the linear region respectively (Fig. 3B). Generally, the bare GCE showed small semicircle region and an almost straight line (Fig. 3B, **curve a**). After adding the MoS_2/Ti_3C_2 nanohybrids onto GCE, the semicircle diameter of Nyquist spectra (Fig. 3B, **curve b**) raised sharply. This trend indicated the electron transfer resistance at the surface increased largely, resulting from the nanohybrids added expanding the gap between the electrode surface and the supporting electrolyte solution and the distance of charge exchange. In contrast, the sorption of AuNPs decreased the semicircle diameter of Nyquist spectra (Fig. 3B, **curve c**). The curve illustrated that R_{ct} values at the electrode surface were decreased, which was consistent with the improvement of electron migration.

CV and EIS experiments were coincident with each other, which claimed the successful modification of MoS_2/Ti_3C_2 nanohybrids and AuNPs. In addtion, the peak of oxidation was chosen to discuss the capability of nanobiosensor in the DPV techniques, resulting from that the peak current ratio ($R_{a/c}$) is about 1.02 (Wu et al., 2012).

3.3. Optimization of biosensing platform for miRNA-182 detection

Concentration of MoS_2/Ti_3C_2 nanohybrids. The amount of MoS_2/Ti_3C_2 nanohybrids was very important and influential during the sensing process. With the increasing amount of MoS_2/Ti_3C_2 nanohybrids, the peak current of redox increased first and was kept or decreased (Fig. 4A). When the concentration of MoS_2/Ti_3C_2 nanohybrids was low, the nanohybrids film was too thin to provide enough active sites to adsorb and immobilize AuNPs. Until the concentration of MoS_2/Ti_3C_2 nanohybrids was up to 1.5 mg/mL, the nanohybrids film was too thick and obstructs the electron transfer between electrode and solution. As shown in the Nyquist spectra (Fig. 4B), the tendency of the slope in the linear region was consistent with the tendency of the peak current of redox appeared in the CV plot. Thus, 1.5 mg/mL was the optimum of miRNA-182 detection.

Probe RNA concentration. The concentration detection of miRNA-182 was depended on the amount of probe RNA immobilized on the electrode surface directly. According to the DPV curves (Fig. 4C), with the increase of probe RNA concentration, the peak current went up until the probe concentration up to 1.0×10^{-9} M. At low probe concentration (less than 1.0×10^{-9} M), the capture efficiency of target miRNA-182 was low because of the immobilization of probe RNA decreasing, resulting in the low peak current of DPV at first. With the increase of probe RNA concentration, the capture efficiency increased so that the peak current went up until the probe concentration up to 1.0×10^{-9} M. When the concentration of probe RNA continuously increasing, the hybridization of target miRNA-182 with immobilized

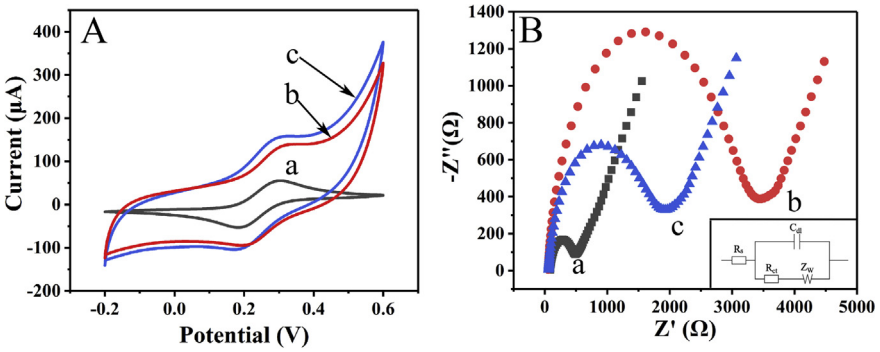

Fig. 3. CV (A) and EIS (B) of bare GCE (a), MoS_2/Ti_3C_2/GCE (b) and AuNPs/MoS_2/Ti_3C_2/GCE (c) in PBS buffer solution (pH 7.4) containing 0.1M KCl and 2.5 mM $[Fe(CN)_6]^{3-/4-}$; the schematic of Randle's equivalent circuit (B-insert).

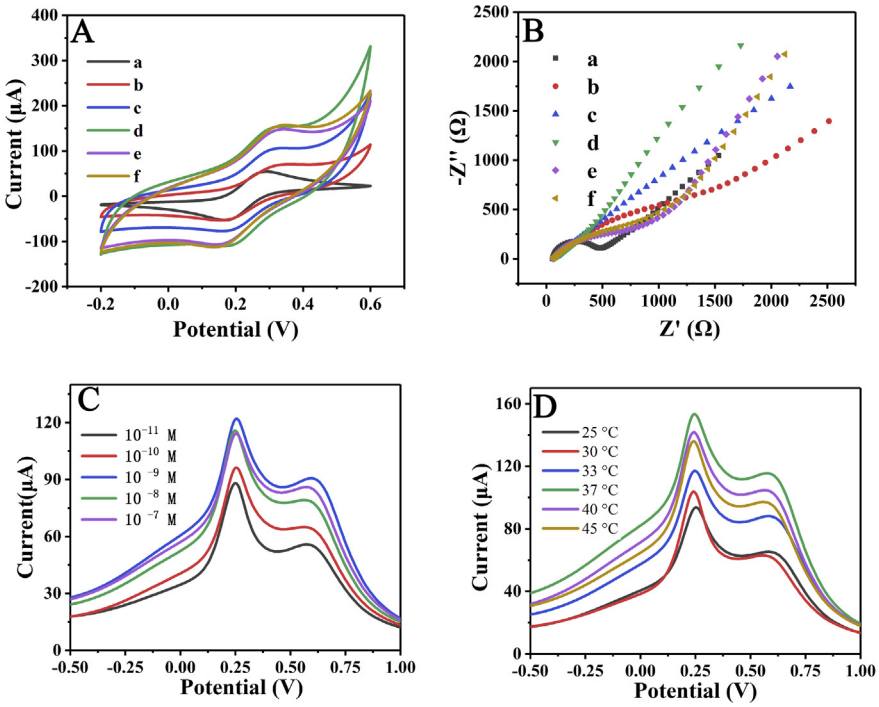

Fig. 4. CV (A) and EIS (B) of AuNPs/MoS_2/Ti_3C_2/GCE modified with different concentrations of MoS_2/Ti_3C_2 nanohybrids (from a to f): including 0 mg/mL, 0.5 mg/mL, 1.0 mg/mL,1.5 mg/mL, 2.0 mg/mL and 2.5 mg/mL; DPV curves responding to 1.0×10^{-12} M miRNA-182 for evaluating the optimization of different parameters influencing detection performance: the concentration of probe RNA (C) and the hybridization temperature (D). All the electrochemical techniques were repeated three times using different GCE and tested in the PBS solution (pH 7.4) containing 0.1M KCl and 2.5 mM $[Fe(CN)_6]^{3-/4-}$.

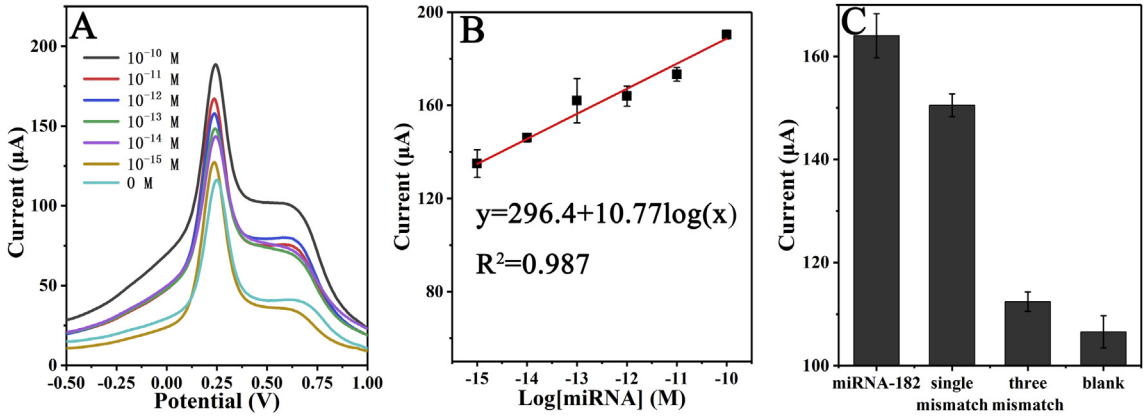

Fig. 5. DPV (A) response of BSA/ssRNA/AuNPs/MoS_2/Ti_3C_2/GCE at various concentration of miRNA-182 (0, 1.0×10^{-15}-1.0×10^{-10} M). Calibration plot (B) between the magnitudes of peak current obtained and log of miRNA-182 concentration. DPV (C) response of the proposed biosensor in selectivity for complementary target miRNA-182, single mismatch miRNA, three mismatch miRNA and blank. The concentration was 1pM respectively. All the electrochemical techniques were repeated three times using different GCE and tested in the PBS solution (pH 7.4) containing 0.1M KCl and 2.5 mM $[Fe(CN)_6]^{3-/4-}$.

Table 1
Comparison of the biosensing performance of Au nanoparticles-grafted MoS_2/Ti_3C_2 nanohybrids constructed in this study against the recently reported biosensors of miRNAs based on MoS_2 nanomaterials.

Materials	Detection methods	Target miRNA	Linear range (M)	LOD (fM)	Ref
polyC10-MB/MoS_2	Fluorescence	miRNA let-7b	10 f-10 p	3.4	Xiao et al. (2018)
MoS_2	Field-effect transistor	miRNA-155	0.1 f-10 n	0.03	Majd et al. (2018)
MoS_2-AuNPs	Photoelectrochemical	miRNA-21	10 f-1 n	4.21	Fu et al. (2018)
AuNPs@MoS_2	DPV	miRNA-21	10 f- 1 n	0.78	Lorencová et al. (2017)
	EIS			0.45	
MoS_2/Ti_3C_2	DPV	miRNA-182	1 f −0.1 n	0.43	This work

probe RNA was saturated and the release of dsRNA was almost invariable. However, the immobilization of probe RNA was increasing, so the residue probe and negative charge on the electrode was increasing. Therefore, the peak current held on or decreased under the coupling effect of the saturation of hybridization and the increasing residue probe when the probe concentration was more than 1.0×10^{-9} M. Hence, the effect of detection was optimal as the probe concentration up to 1.0×10^{-9} M.

Hybridization temperature. The binding degree of probe RNA and miRNA-182 was affected greatly by hybridization temperature, which influences the detection of miRNA-182 (Fig. 4D). The detection was sensible to the temperature change, and the plots illustrates that 37 °C, which was near the human physiological temperature, was the most suitable condition to detect miRNA-182.

3.4. Sensitivity, reproducibility and selectivity for miRNA-182 sensing

The electrochemical measurements of various concentration of miRNA-182 were obtained at the optimal sensing conditions as following: 1.5 mg/mL for MoS_2/Ti_3C_2, 1.0×10^{-9} M for ssRNA and 37 °C for the hybridization of target miRNA-182 with ssRNA. As shown in Fig. 5A, the proposed biosensor exhibited great sensitivity to the concentration change of target miRNA-182. The hybridization of target miRNA-182 with ssRNA causes the swelling-induced Au–S breakage. Then, the negative charge on the surface of electrode decreased, which led to the raise of electron transfer magnitude between electrode and electrolyte. The calibration plot indicates that the average peak current increased linearly against the logarithm concentration of the dropped miRNA-182 (Fig. 5B).

Meanwhile, the extensive application of the biosensors was depended on its reproducibility. Therefore, all the DPV electrochemical measurements have been carried out for three times at least on different GCE to verify the reproducibility of the proposed biosensor. From 10^{-15} M to 10^{-10} M, the corresponding coefficient of variation of the sensing (n = 3) are calculated to be 4.369%, 1.232%, 6.013%, 2.622%, 1.702% and 0.992% separately. The reproducibility of miRNA-182 biosensor was shown in Fig. 5B. The linear relationship in a range of 1 fM to 0.1 nM was depicted by the regression equation:

I_p (μA) = 296.4 + 10.77logC (I: the peak current value; C: the target miRNA-182 concentration and the regression coefficient $R^2 = 0.987$).

Furthermore, the detection limit of 0.43 fM was calculated by X + 3σ (X: the average of the peak current of DPV; σ: the known standard deviation of DPV blank signal consecutive readings). Compared with the reported biosensors, our biosensor is competitive as shown in the Table 1.

The selectivity of the proposed biosensor was obtained by performing the detection of thoroughly complementary miRNA-182, the single-mismatched target miRNA, the three-mismatched target miRNA at 1.0×10^{-12} M respectively (Fig. 5C). The peak current of thoroughly complementary miRNA-182 was the highest among them, and the signal of three-mismatched target miRNA was close to the blank one.

3.5. Stability and serum sample studies

The stability of the proposed biosensor has great influence on its practicability. Therefore, a lifetime study of the biosensor was performed at regular interval of time. The modified electrode was storage at 4 °C for 0–8 days to evaluate its stability. The study showed that a total loss of about 17% appears in signal strength after 8 days. (Fig. S4).

To evaluate the applicability of this sensing strategy in real sample, three different amounts of miRNA-182 have been added into human serums, and detected results shown in Table S1 indicated desired recovery rates and low relative standard deviation (RSD) percentages. The recovery was 105.10%, 95.30% and 92.96% for the concentration of 10^{-10} M, 10^{-12} M and 10^{-14} M respectively, manifesting its effective detection of miRNA-182 in real sample. In addition, the biosensor showed good reproducibility according to the low RSD percentages (Table S1).

4. Conclusion

In summary, MoS_2/Ti_3C_2 nanohybrids have been prepared and applied in the ultrasensitive detection of special miRNA by the comprehensive utilization of Ti_3C_2 frames with layered sturcture and MoS_2 nanoflakes with massive active sites. On one hand, DPV signal is amplified due to the support of MoS_2/Ti_3C_2 nanohybrids and dropped AuNPs; on the other hand, the peak current increases with the swelling-induced Au–S bond breakage due to the huge grafting density after adding miRNA-182. By this way, the linear detection window is determined in a range from 1 fM to 0.1 nM with the detection limit of 0.43 fM. In addtion, the detection of miRNA-182 in serum verifies its well practicability. Now, it is difficult for us to achieve multiplex sensing of kinds of miRNAs synchronously. In the future, more in-depth research will be carred out to realize synchronous multi-channel sensing of kinds of miRNAs based on the strategy suggested in this work.

Declaration of interests

The authors declare that they have no known competing financial interests or personal relationships that could have appeared to influence the work reported in this paper.

The authors declare the following financial interests/personal relationships which may be considered as potential competing interests:

Acknowledgements

This work is financially supported by the National Natural Science Foundation of China (51822501), the Natural Science Funds for Distinguished Young Scholar of Jiangsu Province(BK20170023), the Fundamental Research Funds for the Central Universities (3202009461, 3202009464, 3202009465), the Qing Lan Project of Jiangsu Province, the International Foundation for Science, Stockholm, Sweden, the Organization for the Prohibition of Chemical Weapons, The Hague, Netherlands, through a grant to Lei Liu (F/4736–2), the grants from Top 6 High-Level Talents Program of Jiangsu Province (2017-GDZB-006, Class A), the Natural Science Foundation of Jiangsu Province (BK20181274), the Tribo1ogy Science Fund of State Key Laboratory of Tribology (SKLTKF15A11), Open Research Fund of State Key Laboratory of High Performance Complex Manufacturing, Central South University (Kfkt2016-11), Open Research Fund of State Key Laboratory of Fire Science (HZ2017-KF05) and Open Research Fund of State Key Laboratory of solid lubrication (LSL-1607).

Appendix A. Supplementary data

Supplementary data to this article can be found online at https://doi.org/10.1016/j.bios.2019.04.059.

References

Bray, F., Ferlay, J., Soerjomataram, I., Siegel, R.L., Torre, L.A., Jemal, A., 2018. CA-Canc. J. Clin. 68 (6), 394–424.
Chen, X., Ba, Y., Ma, L., Cai, X., Yin, Y., Wang, K., Guo, J., Zhang, Y., Chen, J., Guo, X., Li, Q., Li, X., Wang, W., Zhang, Y., Wang, J., Jiang, X., Xiang, Y., Xu, C., Zheng, P., Zhang, J., Li, R., Zhang, H., Shang, X., Gong, T., Ning, G., Wang, J., Zen, K., Zhang, J., Zhang, C., 2008. Cell Res. 18 (10), 997.
Chen, Y., Ren, R., Pu, H., Chang, J., Mao, S., Chen, J., 2017. Biosens. Bioelectron. 89, 505–510.
Chia, X., Eng, A.Y.S., Ambrosi, A., Tan, S.M., Pumera, M., 2015. Chem. Rev. 115 (21), 11941–11966.
Dong, H., Zhang, J., Ju, H., Lu, H., Wang, S., Jin, S., Hao, K., Du, H., Zhang, X., 2012. Anal. Chem. 84 (10), 4587–4593.
Fu, N., Hu, Y., Shi, S., Ren, S., Liu, W., Su, S., Zhao, B., Weng, L., Wang, L., 2018. Analyst 143 (7), 1705–1712.
Gan, X., Zhao, H., Quan, X., 2017. Biosens. Bioelectron. 89, 56–71.
Ji, J., Wen, J., Shen, Y., Lv, Y., Chen, Y., Liu, S., Ma, H., Zhang, Y., 2017. J. Am. Chem. Soc. 139 (34), 11698–11701.
Joly-Pottuz, L., Dassenoy, F., Martin, J.M., Vrbanic, D., Mrzel, A., Mihailovic, D., Vogel, W., Montagnac, G., 2005. Tribol. Lett. 18 (3), 385–393.
Kalantar-zadeh, K., Ou, J.Z., 2015. ACS Sens. 1 (1), 5–16.
Kumar, S., Lei, Y., Alshareef, N.H., Quevedo-Lopez, M.A., Salama, K.N., 2018. Biosens. Bioelectron. 121, 243–249.
Li, X.D., Fang, Y.M., Wu, S.Q., Zhu, Z.Z., 2015. AIP Adv. 5 (5), 057143.
Li, Y., Zhang, H., Li, Y., Zhao, C., Fan, Y., Liu, J., Li, X., Liu, H., Chen, J., 2018a. Mol. Carcinog. 57 (1), 125–136.
Li, Y., Zhang, H., Gong, H., Yuan, Y., Li, Y., Wang, C., Li, W., Zhang, Z., Liu, M., Liu, H., Chen, J., 2018b. J. Exp. Clin. Cancer Res. 37 (1), 141.
Lin, H., Wang, X., Yu, L., Chen, Y., Shi, J., 2016a. Nano Lett. 17 (1), 384–391.
Lin, H., Wang, X., Yu, L., Chen, Y., Shi, J., 2016b. Nano Lett. 17 (1), 384–391.
Liu, L., Jiao, S., Peng, Y., Zhou, W., 2018. ACS Sustain. Chem. Eng. 6 (6), 7372–7379.
Lorencová, L., Bertok, T., Dosekova, E., Holazová, A., Paprckova, D., Vikartovská, A., Sasinkova, V., Filip, J., Kasak, P., Jerigova, M., Velic, D., Mahmoud, K., Velic, D., 2017. Electrochim. Acta 235, 471–479.

Lv, B.E., Zhou, Y., Cha, W., Wu, Y., Hu, J., Li, L., Chi, L., Ma, H., 2014. ACS Appl. Mater. Interfaces 6 (11), 8313–8319.
Majd, S.M., Salimi, A., Ghasemi, F., 2018. Biosens. Bioelectron. 105, 6–13.
Mikhlin, Y., Likhatski, M., Tomashevich, Y., Romanchenko, A., Erenburg, S., Trubina, S., 2010. J. Electron. Spectrosc. 177 (1), 24–29.
Miko, E., Czimmerer, Z., Csánky, E., Boros, G., Buslig, J., Dezső, B., Scholtz, B., 2009. Exp. Lung Res. 35 (8), 646–664.
Naguib, M., Kurtoglu, M., Presser, V., Lu, J., Niu, J., Heon, M., Hultman, L., Gogotsi, Y., Barsoum, M.W., 2011. Adv. Mater. 23 (37), 4248–4253.
Panagopoulou, M.A., Stergiou, D.V., Roussis, I.G., Prodromidis, M.I., 2010. Anal. Chem. 82 (20), 8629–8636.
Resnick, K.E., Alder, H., Hagan, J.P., Richardson, D.L., Croce, C.M., Cohn, D.E., 2009. Gynecol. Oncol. 112 (1), 55–59.
Roointan, A., Mir, T.A., Wani, S.I., Hussain, K.K., Ahmed, B., Abrahim, S., Savardashtaki, A., Gandomani, G., Gandomani, M., Chinnappan, R., Akhtar, M.H., 2018. J. Pharm. Biomed.
Rupaimoole, R., Slack, F.J., 2017. Nat. Rev. Drug Discov. 16 (3), 203.
Ryoo, S.R., Lee, J., Yeo, J., Na, H.K., Kim, Y.K., Jang, H., Lee, J., Han, S., Lee, Y., Kim, V., Min, D.H., 2013. ACS Nano 7 (7), 5882–5891.
Shuai, H.L., Huang, K.J., Chen, Y.X., Fang, L.X., Jia, M.P., 2017. Biosens. Bioelectron. 89, 989–997.
Suni, I.I., 2008. Trac. Trends Anal. Chem. 27 (7), 604–611.
Tan, C., Cao, X., Wu, X.J., He, Q., Yang, J., Zhang, X., Chen, J., Zhao, W., Han, S., Nam, G., Sindoro, M., Zhang, H., 2017. Chem. Rev. 117 (9), 6225–6331.
Tian, L., Qian, K., Qi, J., Liu, Q., Yao, C., Song, W., Wang, Y., 2018. Biosens. Bioelectron. 99, 564–570.
Wu, S., Zeng, Z., He, Q., Wang, Z., Wang, S.J., Du, Y., Yin, Z., Sun, X., Chen, W., Zhang, H., 2012. Small 8 (14), 2264–2270.
Xiao, M., Chandrasekaran, A.R., Ji, W., Li, F., Man, T., Zhu, C., Shen, X., Pei, H., Li, Q., Li, L., 2018. ACS Appl. Mater. Interfaces 10 (42), 35794–35800.
Zhang, W., Dai, Z., Liu, X., Yang, J., 2018. Biosens. Bioelectron. 105, 116–120.
Zhao, H., Shen, J., Medico, L., Wang, D., Ambrosone, C.B., Liu, S., 2010. PLoS One 5 (10), e13735.
Zhu, W., Liu, X., He, J., Chen, D., Hunag, Y., Zhang, Y.K., 2011. BMC Canc. 11 (1), 393.